

Hierarchical Federated Learning with SignSGD: A Highly Communication-Efficient Approach

Amirreza Kazemi, Seyed Mohammad Azimi-Abarghouyi, *Member, IEEE*, Gabor Fodor, *Fellow, IEEE*, and Carlo Fischione, *Fellow, IEEE*

Abstract—Hierarchical federated learning (HFL) has emerged as a key architecture for large-scale wireless and Internet of Things systems, where devices communicate with nearby edge servers before reaching the cloud. In these environments, uplink bandwidth and latency impose strict communication limits, thereby making aggressive gradient compression essential. One-bit methods such as sign-based stochastic gradient descent (SignSGD) offer an attractive solution in flat federated settings, but existing theory and algorithms do not naturally extend to hierarchical settings. In particular, the interaction between majority-vote aggregation at the edge layer and model aggregation at the cloud layer, and its impact on end-to-end performance, remains unknown. To bridge this gap, we propose a highly communication-efficient sign-based HFL framework and develop its corresponding formulation for nonconvex learning, where devices send only signed stochastic gradients, edge servers combine them through majority-vote, and the cloud periodically averages the obtained edge models, while utilizing downlink quantization to broadcast the global model. We introduce the resulting scalable HFL algorithm, HierSignSGD, and provide the convergence analysis for SignSGD in a hierarchical setting. Our core technical contribution is a characterization of how biased sign compression, two-level aggregation intervals, and inter-cluster heterogeneity collectively affect convergence. Numerical experiments under homogeneous and heterogeneous data splits show that HierSignSGD, despite employing extreme compression, achieves accuracy comparable to or better than full-precision stochastic gradient descent while reducing communication cost in the process, and remains robust under aggressive downlink sparsification.

Index Terms—Hierarchical federated learning, majority-vote, quantization, SignSGD.

I. INTRODUCTION

Federated learning (FL) allows distributed devices to collaboratively train a global model without sharing raw data, reducing privacy risks. This approach is particularly advantageous when data is expensive to collect or challenging to aggregate. Moreover, FL enhances computational efficiency by allowing multiple devices to train the model concurrently [1].

Despite its advantages, the standard FL paradigm struggles with scalability. As the number of participating devices grows, communication rounds become progressively slower, uplink congestion increases, and stragglers increasingly dominate the overall round latency. To address these issues, numerous works in FL have introduced modified algorithms aimed at mitigating the effects of the aforementioned challenges [2]–[5].

The authors are with the School of Electrical Engineering and Computer Science, KTH Royal Institute of Technology, Stockholm, Sweden (Emails: {seykaz, seyyaa, gaborf, carlofi}@kth.se). This research has received funding from the European Union’s Horizon Europe research project BATTwin under grant agreement No. 101137954.

A recent structural evolution of the standard FL framework is hierarchical federated learning (HFL), in which devices send their updates to intermediate edge servers rather than directly to the cloud server [6]–[9]. In its typical form, HFL employs a two-stage aggregation process: edge servers first combine updates from their associated devices, and the cloud then aggregates the outputs of multiple edge servers to obtain the global model. By introducing this intermediate layer, HFL has the potential to reduce communication load, improve scalability, and enable more efficient distributed learning in large-scale networks.

Notwithstanding its benefits, HFL continues to face a critical bottleneck involving uplink communication between devices and edge servers. Transmitting full-precision gradients or model updates is costly, especially over noisy or bandwidth-constrained communication links where frequent two-way transmissions take place. As a result, communication-efficient learning techniques have become indispensable for HFL systems. Most existing studies in FL and HFL improve communication efficiency by applying general quantization to model parameters or gradients during uplink transmission.

While such schemes reduce communication costs, they still require multiple bits per model dimension, which can be prohibitive due to the scale of modern learning models, even with a modest number of devices. This limitation typically occurs in settings constrained by bandwidth, latency, or energy, such as large-scale Internet of Things deployments with severely limited uplink rates [10], [11], wireless edge-learning systems under stringent bandwidth budgets [12], [13], and distributed sensor networks, such as in fault prediction in factories (e.g., for electrical battery manufacturing processes or industrial automation processes), where nodes can transmit only a few bits per reporting cycle [14]. The challenge is further amplified in emerging applications involving large language models, where adding even a single extra bit per dimension substantially increases the communication load, rendering multi-bit schemes ineffective and making one-bit, sign-based methods particularly attractive.

A promising way to achieve this goal is to apply aggressive compression to the transmitted updates. In this context, sign-based stochastic gradient descent (SignSGD) is especially appealing because each device sends only the coordinate-wise signs of its stochastic gradients rather than full-precision values. This reduces the uplink payload of each device from d floats to d bits (d being the dimension of the model). To appreciate the magnitude of this reduction, consider the baseline in which devices transmit full-precision 32-bit model

TABLE I
COMPARISON OF PROMINENT EXISTING WORKS IN HFL

Work	Convergence analysis	Communication efficiency	Inter-cluster heterogeneity	Downlink quantization
[7]	✓	✓	✗	✗
[8]	✗	✗	✗	✗
[9]	✓	✓	✓	✗
[15]	✓	✗	✓	✗
[16]	✓	✓	✗	✗
This work	✓	✓	✓	✓

parameters. Using a sparsifier, for example, to match the communication budget of SignSGD would require retaining only 2–3% of the parameter entries via sparsification. Such extreme compression is prone to instability and often degrades convergence due to the significant variance it introduces [7], [17], as it discards essential information contained in the entries. But the directional information of gradients can be somewhat preserved even when reduced to a single bit per coordinate. This makes sign-based gradient communication particularly well suited for federated systems with severe communication constraints. Moreover, SignSGD can be viewed as a form of quantization possessing a fundamentally different and unique characterization that cannot be captured by the general or specific quantization schemes widely studied in many FL works [18]. In particular, existing quantization-based methods typically rely on simple statistical characterizations, such as modeling quantization error through its mean and variance, which makes their incorporation into convergence analysis relatively straightforward, since the quantization error appears as an additive noise term. In contrast, SignSGD requires a highly delicate, integer-based analysis, as its behavior is governed by sign operations and majority-vote mechanisms rather than additive quantization noise. Such treatment necessitates a new theoretical and analytical framework in HFL that is fundamentally different from those used in previous works.

Early works studied SignSGD in the classical distributed stochastic gradient descent (SGD) context, showing that even though the sign is a biased operator, convergence (in homogeneous or well-controlled settings) to stationary points is feasible under suitable assumptions [18]–[20]. More recent advances improve these results via variance reduction to tighten convergence bounds in nonconvex settings [21], [22]. Moreover, momentum variants of SignSGD have been shown to enjoy convergence under weaker smoothness conditions [23]. However, nearly all of the literature on SignSGD and especially its variants assumes the standard flat (device–server) communication topology, while in many real-world settings, networks naturally follow multi-layer hierarchical architectures [24], [25].

To combine the strengths of SignSGD and HFL, SignSGD can be adopted as the backbone of device–edge communication updates, complementing hierarchical clustering and resulting in a highly communication-efficient framework not achieved by existing methods. However, realizing this potential requires a rigorous mathematical formulation of the hierarchical learning process, together with a concrete characterization of the underlying algorithm and a convergence analysis that accurately reflects real-world operating conditions. Developing

such a modeling framework and providing its corresponding theoretical analysis constitute the main goals of this work.

A. Related Works and Challenges

In contrast to the extensive literature on standard FL, research on hierarchical FL remains relatively sparse. For example, [7] analyzes a HFL algorithm with quantization, proving a tight convergence bound under nonconvex objectives and deriving system-design insights such as adaptive aggregation intervals and device–edge association strategies, though the analytical results do not sufficiently cover non-IID distributions and downlink quantization. Another study [8] develops a HFL algorithm derived from a different optimization perspective, yet the convergence guarantees offered are limited to a special case.

A related line of work is presented in [9], which examines HFL under quantized communication and heterogeneous data, providing an analysis of convergence behavior and identifying aggregation intervals that improve communication efficiency and learning accuracy, although only uplink quantization is considered. Extensions to multi-layer HFL with layer-specific quantization more recently generalize hierarchical FL theory to deeper aggregation graphs and show how local iteration counts and quantization parameters should scale [26]. Separately, the recent work [15] gives a unified convergence framework for HFL under partial participation and data heterogeneity, without utilizing quantization.

A different strategy for easing communication burdens is model pruning [16], which reduces the number of transmitted parameters by eliminating redundant ones, thereby lowering communication costs without significantly affecting model accuracy. Multiple studies have also explored the combination of HFL with over-the-air computation [27]–[29], where it is shown that analog aggregation and hierarchical clustering can greatly improve scalability and strengthen robustness to interference and data heterogeneity in wireless networks. Additionally, context-aware and scheduling-driven frameworks [30], [31] dynamically manage device participation and communication resources, enabling more flexible and stable training.

To improve scalability and reduce deployment overhead, prior work has also studied clustering and aggregator-placement strategies [32], [33]. Meanwhile, heterogeneity-aware client association and staleness control methods [34] aim to strengthen convergence in practical network settings. While these works introduce valuable methods for HFL, they also exhibit limitations tied to key challenges such as incomplete convergence analysis, restricted bandwidth, and data heterogeneity (see Table I for an overview). A recurring issue

is the underutilization of quantization, as many approaches apply it only to the uplink rather than to both communication phases. Furthermore, data heterogeneity, especially across devices linked to different edge servers, adds another layer of difficulty, since in realistic deployments devices often hold substantially different data distributions.

Contributions

To our knowledge, this is the first work to provide a complete framework design and analysis of SignSGD within a HFL architecture while accounting for practical inter-edge non-IID data distributions and downlink quantization during model broadcast. It further appears to be the only HFL study that supports fully binary communication in both the uplink and downlink between edge servers and their device clusters. This feature is particularly noteworthy as it allows devices to operate with extremely limited information exchange over any given modulation. Our main contributions are outlined below.

- We propose HierSignSGD, the first fully sign-based training framework for HFL. Devices organized into any number of clusters transmit only the signs of their stochastic gradients, edge servers aggregate these updates via clustered majority-vote, and the cloud periodically averages edge models. To achieve additional communication savings, we extend the algorithm to support quantized downlink broadcasts using stochastic compression, for which we also provide an analysis and establish the corresponding convergence guarantee.
- Our nonconvex convergence analysis explicitly quantifies how the two aggregation intervals (edge and cloud) and the degree of heterogeneity influence the convergence bound, in contrast to existing analyses of SignSGD-based methods, which are notably simpler and limited to the conventional single-cluster (flat) architecture. Furthermore, under specific conditions HierSignSGD converges to a first-order stationary point for nonconvex objectives at a sublinear rate of $\mathcal{O}(1/\sqrt{T_G})$, where T_G denotes the number of global rounds. Notably, the bound exhibits a nonmonotonic dependence on the number of edge-device communication steps, indicating the presence of an optimal setting, an effect further examined in our experiments under both IID and non-IID data distributions.
- Numerical experiments under different settings demonstrate that HierSignSGD achieves accuracy comparable to or exceeding that of full-precision hierarchical SGD, while delivering substantial communication savings. When examining different clustering configurations, we find that a hierarchical setup does in fact offer a notable improvement in convergence speed over a flat FL design. Moreover, the effect of edge-device communication rounds is investigated to confirm the practical relevance of the theoretical predictions. The proposed algorithm also remains robust under aggressive downlink sparsification.

The rest of the paper is organized as follows. Section II introduces the HFL framework, formalizes the global and edge-level objectives, and discusses the communication constraints

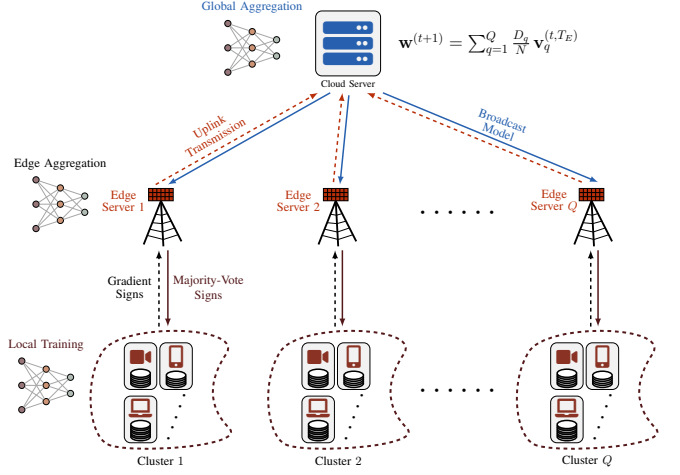


Fig. 1. SignSGD-based implementation for a HFL scenario; devices send gradient signs to their edge servers, the servers broadcast majority-vote results back; after several rounds, the edge servers forward the model parameters to final aggregation.

that motivate sign-based optimization. Section III presents the proposed HierSignSGD algorithm in detail and provides the convergence analysis, where we derive bounds under smoothness, bounded variance, and gradient dissimilarity assumptions, and extend the results to downlink quantization. Section IV presents numerical results evaluating the convergence behavior and robustness of the method.

Notations: Throughout the text, we use bold lowercase letters and italic letters to indicate vectors and scalars, respectively. $[\mathbf{a}]_i$ is the i th element of \mathbf{a} . The operator $\text{sgn}(\cdot)$ represents the element-wise sign function. A vector norm and its dual are denoted by $\|\cdot\|$ and $\|\cdot\|_*$, respectively. The inner product of two vectors is expressed by $\langle \cdot, \cdot \rangle$. The expectation operator is denoted by $\mathbb{E}\{\cdot\}$, though for brevity, we may occasionally denote the expectation by $\overline{\{\cdot\}}$. For any function f , ∇f indicates its gradient. The hat notation $\hat{(\cdot)}$ denotes an estimate of a given variable. $\mathbf{1}_p$ represents the all-one vector. $\mathcal{Z}(\cdot)$ represents a stochastic quantization operator. Also, see Table II for a more detailed summary of the notation and symbols used throughout the paper.

II. THE HFL PROBLEM

The hierarchical structure typically consists of two layers. The first (or top) layer enables communication between the cloud server and the edge servers, which function as intermediate aggregators. This layer is responsible for transmitting model parameters for the purpose of global aggregation. The second layer establishes connections between edge devices and their corresponding edge servers. Over the communication channel in this layer, devices exchange privacy-preserving updates with their edge servers, which then update the local models accordingly. This process mirrors the behavior of a conventional FL framework. We assume that communication between edge servers and the cloud server takes place over high-capacity backhaul links and is therefore ideal, leaving the device-edge uplink as the primary communication bottleneck.

TABLE II
SUMMARY OF IMPORTANT NOTATIONS

Symbol	Description
Q	Number of edge servers
\mathcal{V}^q	Set of devices managed by edge server q
\mathcal{D}_{qk}	Dataset belonging to device k of cluster q
$ \mathcal{D}_{qk} $	Size of the local dataset
D_q	Number of data samples belonging to cluster q
N	Total number of samples in the hierarchical network
d	Dimension of the model parameter vector
\mathbf{w}	Global model parameter vector
$\mathcal{L}(\mathbf{w}; \xi)$	Loss function for a single sample vector ξ
$f_{qk}(\mathbf{w})$	Local loss function of device k of cluster q
$\mathcal{F}_q(\mathbf{w})$	Loss function at edge server q
$\mathcal{F}(\mathbf{w})$	Global loss function
T_G	Number of global rounds
T_E	Number of local iterations per global round
t	Index of global updates
τ	Index of local updates
$\mathbf{w}^{(t)}$	Global model at iteration t
$\mathbf{v}_q^{(t, \tau)}$	Edge model q at iteration (t, τ)
$\hat{\mathbf{g}}_{qk}^{(t, \tau)}$	Stochastic gradient estimated by device k of cluster q
$\mathbf{s}_q^{(t, \tau)}$	Majority-vote gradient at edge q
μ	step-size
B	batch-size
L	The smoothness constant
σ^2	Gradient component variance bound
ζ	Gradient dissimilarity constant
ψ	Quantizer bound coefficient

For our configuration, depicted in Fig. 1, we assume that the cloud server manages Q edge servers, each of which is connected to its cluster of devices. For edge server q , we denote the device set by \mathcal{V}^q . Device k in \mathcal{V}^q has access to the local dataset \mathcal{D}_{qk} , which it uses to train its local learning model. Let us denote the loss function for a single sample as $\mathcal{L}(\mathbf{w}; \xi)$ where \mathbf{w} is the model parameter vector and ξ is the sample vector containing the input and output values. Based on this, the local average loss function device k belonging to edge server q is

$$f_{qk}(\mathbf{w}) = \frac{1}{|\mathcal{D}_{qk}|} \sum_{\xi \in \mathcal{D}_{qk}} \mathcal{L}(\mathbf{w}; \xi). \quad (1)$$

Accordingly, the global average loss function is defined as

$$\mathcal{F}(\mathbf{w}) \triangleq \frac{1}{N} \sum_{q=1}^Q \sum_{k \in \mathcal{V}^q} \sum_{\xi \in \mathcal{D}_{qk}} \mathcal{L}(\mathbf{w}; \xi), \quad (2)$$

where N is the total number of data samples in the network. However, it is beneficial to reformulate $\mathcal{F}(\mathbf{w})$ in a way that mirrors the hierarchical format illustrated earlier. To this end, consider the edge loss functions

$$\mathcal{F}_q(\mathbf{w}) = \sum_{k \in \mathcal{V}^q} \frac{|\mathcal{D}_{qk}|}{D_q} f_{qk}(\mathbf{w}), \quad (3)$$

where $D_q = \sum_{k \in \mathcal{V}^q} |\mathcal{D}_{qk}|$. It is evident that (2) can now be equivalently recast as

$$\mathcal{F}(\mathbf{w}) = \sum_{q=1}^Q \frac{D_q}{N} \mathcal{F}_q(\mathbf{w}), \quad (4)$$

which is a hierarchical representation of the global loss function, as intended.

The ultimate goal is to minimize $\mathcal{F}(\mathbf{w})$:

$$\mathbf{w}^* = \arg \min_{\mathbf{w}} \mathcal{F}(\mathbf{w}). \quad (5)$$

A typical solution for finding \mathbf{w}^* is to use the SGD approach with step-size μ :

$$\begin{aligned} \mathbf{w} &\leftarrow \mathbf{w} - \mu \nabla \mathcal{F}(\mathbf{w}) = \mathbf{w} - \mu \sum_{q=1}^Q \frac{D_q}{N} \nabla \mathcal{F}_q(\mathbf{w}) \\ &\Leftrightarrow \mathbf{w} \leftarrow \sum_{q=1}^Q \frac{D_q}{N} (\mathbf{w} - \mu \nabla \mathcal{F}_q(\mathbf{w})), \end{aligned} \quad (6)$$

where the last representation implies that the edge servers can execute the gradient descent iteration locally and send the parameter models to the cloud server for global aggregation, an approach first adopted by the original FL study [1]. Furthermore, from (3) we have

$$\nabla \mathcal{F}_q(\mathbf{w}) = \sum_{k \in \mathcal{V}^q} \frac{|\mathcal{D}_{qk}|}{D_q} \nabla f_{qk}(\mathbf{w}), \quad (7)$$

which indicates that edge servers aggregate the local gradient vectors received from their associated devices, where each device, for the sake of computational efficiency, estimates its gradient using only a small random batch of data samples.

Steps (6) and (7) constitute the core of HFL algorithms; however, we encounter specific challenges when executing the second step. In particular, transmitting distinct gradient values from multiple devices to an edge server over a multiple-access channel places considerable strain on communication resources, such as bandwidth, thereby necessitating some form of data quantization. An extreme form of vector quantization preserves only the signs of the entries, discarding all magnitude information. This leads to the SignSGD update rule. In the following section, we introduce our proposed algorithm, which adopts this highly compressed scheme as part of the edge-device training process.

III. THE HierSignSGD ALGORITHM

In this section, we introduce the proposed HFL algorithm, HierSignSGD. We begin with an overview of the algorithm, followed by a detailed convergence analysis.

A. Pseudocode

The core idea behind HierSignSGD is to implement a hierarchical training procedure that operates efficiently under the stringent communication constraints of the edge–device channel. The pseudocode is provided in Algorithm 1, and a stepwise summary is given below:

- 1) **Broadcast to edges:** At each global round t , the cloud server broadcasts $\mathbf{w}^{(t)}$ to all edge servers.
- 2) **Initializing device model:** Each edge server broadcasts the provided $\mathbf{w}^{(t)}$ to its associated devices, which then set

$$\mathbf{v}_q^{(t,0)} = \mathbf{w}^{(t)}.$$

- 3) **Local gradient computation at devices:** For each local round τ , each device computes a stochastic gradient estimate

$$\hat{\mathbf{g}}_{qk}^{(t,\tau)} = \hat{\nabla} f_{qk}(\mathbf{v}_q^{(t,\tau)}).$$

Then, only the element-wise signs $\text{sgn}(\hat{\mathbf{g}}_{qk}^{(t,\tau)})$ are sent to the corresponding edge server.

- 4) **Vote-based aggregation at edges:** Each edge server aggregates the received signs via a majority-vote

$$\mathbf{s}_q^{(t,\tau)} = \text{sgn} \left(\sum_{k \in \mathcal{V}^q} \text{sgn}(\hat{\mathbf{g}}_{qk}^{(t,\tau)}) \right),$$

and transmits the resulting sign vector back to the devices. Subsequently, both the edge server and the devices update their local models using a sign-based descent step:

$$\mathbf{v}_q^{(t,\tau+1)} = \mathbf{v}_q^{(t,\tau)} - \mu \mathbf{s}_q^{(t,\tau)}.$$

- 5) **Return to cloud and global aggregation:** After T_E local steps at the edge, each edge server sends its final local model $\mathbf{v}_q^{(t,T_E)}$ back to the cloud server for the weighted model aggregation:

$$\mathbf{w}^{(t+1)} = \sum_{q=1}^Q \frac{D_q}{N} \mathbf{v}_q^{(t,T_E)}.$$

We note that the use of sign-based updates to train edge models across multiple clusters directly influences the convergence behavior of the algorithm. A key objective of the following analysis is to characterize how this extreme form of compression, repeatedly applied over multiple edge–device communication rounds, impacts the convergence of HierSignSGD.

Algorithm 1 HierSignSGD

- 1: **Input:** number of global rounds T_G , local steps T_E , step-size μ ; relative edge dataset sizes D_q/N ;
- 2: Initialize global model $\mathbf{w}^{(0)}$;
- 3: **for** $t = 0, 1, \dots, T_G - 1$ **do**
- 4: Broadcast $\mathbf{w}^{(t)}$ to all edge servers;
- 5: **for all** edge servers $q \in \{1, \dots, Q\}$ **in parallel do**
- 6: Broadcast $\mathbf{w}^{(t)}$ to all $k \in \mathcal{V}^q$ for them to set
- 7: $\mathbf{v}_q^{(t,0)} = \mathbf{w}^{(t)};$
- 8: **for** $\tau = 0, 1, \dots, T_E - 1$ **do**
- 9: **for all** devices $k \in \mathcal{V}^q$ **in parallel do**
- 10: $\hat{\mathbf{g}}_{qk}^{(t,\tau)} = \hat{\nabla} f_{qk}(\mathbf{v}_q^{(t,\tau)});$
- 11: Send $\text{sgn}(\hat{\mathbf{g}}_{qk}^{(t,\tau)})$ to edge server q ;
- 12: Compute $\mathbf{s}_q^{(t,\tau)} = \text{sgn} \left(\sum_{k \in \mathcal{V}^q} \text{sgn}(\hat{\mathbf{g}}_{qk}^{(t,\tau)}) \right);$
- 13: Send back $\mathbf{s}_q^{(t,\tau)}$ to the devices;
- 14: Jointly update $\mathbf{v}_q^{(t,\tau+1)} = \mathbf{v}_q^{(t,\tau)} - \mu \mathbf{s}_q^{(t,\tau)};$
- 15: Send $\mathbf{v}_q^{(t,T_E)}$ back to the cloud server;
- 16: **Output:** final global model parameter $\mathbf{w}^{(T_G)}$;

B. Convergence Analysis

We now aim to analyze the convergence of the proposed HierSignSGD algorithm. The main objective is to characterize the expected asymptotic behavior of the iterates $\mathbf{w}^{(t)}$ produced by the algorithm. We do this by providing an upper bound for

$$\mathbb{E} \left\{ \frac{1}{T_G} \sum_{t=0}^{T_G-1} \|\nabla \mathcal{F}(\mathbf{w}^{(t)})\|_1 \right\}, \quad (8)$$

and inspecting what happens to the bound when $T_G \rightarrow \infty$ under certain circumstances. As can be seen, we employ the ℓ_1 norm in (8), and in other parts of the paper we may use different norms. Because we mostly deal with inequalities in our analysis, the choice of norm is inconsequential, as all norms on a finite-dimensional space are equivalent [35]. Hence, we select norms solely for analytical convenience, without loss of generality in the results.

The main assumptions for our analysis, which are common in the FL literature, are the following:

- **A1) Global minimum:** For all $\mathbf{w} \in \mathbb{R}^d$, we have

$$\mathcal{F}(\mathbf{w}) \geq \mathcal{F}^*,$$

where \mathcal{F}^* is the global minimum.

- **A2) Smoothness:** Each loss function $\mathcal{F}_q : \mathbb{R}^d \rightarrow \mathbb{R}$ is L -smooth with respect to $\|\cdot\|$:

$$\|\nabla \mathcal{F}_q(\mathbf{v}) - \nabla \mathcal{F}_q(\mathbf{w})\|_* \leq L \|\mathbf{v} - \mathbf{w}\|, \quad \forall \mathbf{w}, \mathbf{v} \in \mathbb{R}^d,$$

or equivalently

$$\mathcal{F}_q(\mathbf{v}) \leq \mathcal{F}_q(\mathbf{w}) + \langle \nabla \mathcal{F}_q(\mathbf{w}), \mathbf{v} - \mathbf{w} \rangle + \frac{L}{2} \|\mathbf{v} - \mathbf{w}\|^2.$$

Consequently, the global loss function \mathcal{F} in (4) will also possess this property.

- **A3) Bounded variance:** Each stochastic gradient obtained from a random sample is an unbiased estimator of the full-batch gradient, with its coordinates having bounded variance:

$$\mathbb{E}\{\hat{\mathbf{g}}(\mathbf{w})\} = \mathbf{g}(\mathbf{w}), \quad \mathbb{E}\{([\hat{\mathbf{g}}(\mathbf{w})]_i - [\mathbf{g}(\mathbf{w})]_i)^2\} \leq \sigma^2.$$

It follows from this assumption that the mini-batch gradient estimate is also unbiased, with variance bound reduced to σ^2/B , where B denotes the batch-size. By employing the identity $\mathbb{E}\{X\} \leq \sqrt{\mathbb{E}\{X^2\}}$, we deduce

$$\mathbb{E}\{|\hat{\mathbf{g}}(\mathbf{w})]_i - [\mathbf{g}(\mathbf{w})]_i|\} \leq \frac{\sigma}{\sqrt{B}}.$$

- **A4) Local gradient dissimilarity:** We have $\forall \mathbf{w} \in \mathbb{R}^d$

$$\mathbb{E}_{\xi \sim \mathcal{D}} \left\{ \sum_{q=1}^Q \frac{D_q}{N} \|\nabla \mathcal{F}_q(\mathbf{w}) - \nabla \mathcal{F}(\mathbf{w})\|_1 \right\} \leq \zeta,$$

where expectation is taken over the randomness of the device-level data samples. This assumption measures the discrepancy between the local and global gradients. Interestingly, ζ is a quantity that is also called degree of non-IID (see, e.g., [36], [37] and the references therein). In the case where data is balanced equally among the device clusters, then $D_q/N = 1/Q$.

Given assumptions A1–A4, we proceed to analyze the convergence properties of the HierSignSGD algorithm. We first analyze a simplified variant of the algorithm that omits the majority-vote mechanism. We then extend the analysis to demonstrate that the same error bound holds when majority voting is employed at the edge servers.

Theorem 1. Consider running Algorithm 1 with single-device clusters for T_G global iterations and T_E local iterations, using step-size μ and batch-size B . Under assumptions A1–A4, the following performance bound holds:

$$\frac{1}{T_G} \sum_{t=0}^{T_G-1} \mathbb{E}\{\|\nabla \mathcal{F}(\mathbf{w}^{(t)})\|_1\} \leq \frac{\mathcal{F}(\mathbf{w}^{(0)}) - \mathcal{F}^*}{\mu T_G T_E} + C, \quad (9)$$

where

$$C = 2\zeta + \frac{2\sigma d}{\sqrt{B}} + \left(\frac{3T_E}{2} - 1\right)L\mu.$$

Proof. Since there is only one client per server, we can drop the index k for local variables. We start by expressing the $(t+1)$ th global average as

$$\begin{aligned} \mathbf{w}^{(t+1)} &= \sum_{q=1}^Q \frac{D_q}{N} \mathbf{v}_q^{(t, T_E)} \\ &= \sum_{q=1}^Q \frac{D_q}{N} \left(\mathbf{v}_q^{(t, 0)} - \mu \sum_{\tau=0}^{T_E-1} \text{sgn}(\hat{\mathbf{g}}_q^{(t, \tau)}) \right) \\ &= \sum_{q=1}^Q \frac{D_q}{N} \left(\mathbf{w}^{(t)} - \mu \sum_{\tau=0}^{T_E-1} \text{sgn}(\hat{\mathbf{g}}_q^{(t, \tau)}) \right) \\ &= \mathbf{w}^{(t)} - \mu \sum_{q=1}^Q \sum_{\tau=0}^{T_E-1} \frac{D_q}{N} \text{sgn}(\hat{\mathbf{g}}_q^{(t, \tau)}). \end{aligned} \quad (10)$$

Employing assumption A2 with ℓ_∞ norm, we write

$$\begin{aligned} \mathcal{F}(\mathbf{w}^{(t+1)}) - \mathcal{F}(\mathbf{w}^{(t)}) &\leq \left\langle \nabla \mathcal{F}(\mathbf{w}^{(t)}), \mathbf{w}^{(t+1)} - \mathbf{w}^{(t)} \right\rangle \\ &\quad + \frac{L}{2} \left\| \mathbf{w}^{(t+1)} - \mathbf{w}^{(t)} \right\|_\infty^2 \end{aligned} \quad (11)$$

$$\begin{aligned} &= - \left\langle \nabla \mathcal{F}(\mathbf{w}^{(t)}), \mu \sum_{q=1}^Q \sum_{\tau=0}^{T_E-1} \frac{D_q}{N} \text{sgn}(\hat{\mathbf{g}}_q^{(t, \tau)}) \right\rangle \\ &\quad + \frac{L}{2} \left\| \mu \sum_{q=1}^Q \sum_{\tau=0}^{T_E-1} \frac{D_q}{N} \text{sgn}(\hat{\mathbf{g}}_q^{(t, \tau)}) \right\|_\infty^2. \end{aligned} \quad (12)$$

We first bound the second term in (12) by using the triangle inequality as

$$\begin{aligned} &\frac{L}{2} \mu^2 \left\| \sum_{q=1}^Q \sum_{\tau=0}^{T_E-1} \frac{D_q}{N} \text{sgn}(\hat{\mathbf{g}}_q^{(t, \tau)}) \right\|_\infty^2 \\ &\leq \frac{L}{2} \mu^2 \left(\sum_{q=1}^Q \sum_{\tau=0}^{T_E-1} \frac{D_q}{N} \right)^2 = \frac{L}{2} (\mu T_E)^2. \end{aligned} \quad (13)$$

We now proceed to bound the more challenging first term of (12). Let us rewrite the inner product as

$$\begin{aligned} &- \left\langle \nabla \mathcal{F}(\mathbf{w}^{(t)}), \mu \sum_{q=1}^Q \sum_{\tau=0}^{T_E-1} \frac{D_q}{N} \text{sgn}(\hat{\mathbf{g}}_q^{(t, \tau)}) \right\rangle \\ &= - \mu \sum_{q=1}^Q \frac{D_q}{N} \sum_{\tau=0}^{T_E-1} \left\langle \nabla \mathcal{F}(\mathbf{w}^{(t)}), \text{sgn}(\hat{\mathbf{g}}_q^{(t, \tau)}) \right\rangle. \end{aligned} \quad (14)$$

For convenience, we temporarily adopt the following notational switches:

$$\begin{aligned} \nabla \mathcal{F}(\mathbf{w}^{(t)}) &\rightarrow \nabla \mathcal{F}, \quad \nabla \mathcal{F}_q(\mathbf{w}^{(t)}) \rightarrow \nabla \mathcal{F}_q, \\ \hat{\mathbf{g}}_q^{(t, \tau)} &\rightarrow \hat{\mathbf{g}}^{(\tau)}, \quad \mathbf{v}_q^{(t, \tau)} \rightarrow \mathbf{v}^{(\tau)}. \end{aligned} \quad (15)$$

The goal is to bound $-\sum_{\tau=0}^{T_E-1} \langle \nabla \mathcal{F}, \text{sgn}(\hat{\mathbf{g}}^{(\tau)}) \rangle$. Let us denote this by Ω . Guided by the analytical framework of [18], we recast this term as

$$\begin{aligned} \Omega &\triangleq - \sum_{\tau=0}^{T_E-1} \left\langle \nabla \mathcal{F}, \text{sgn}(\hat{\mathbf{g}}^{(\tau)}) \right\rangle = \sum_{\tau=0}^{T_E-1} \left(-\|\nabla \mathcal{F}\|_1 \right. \\ &\quad \left. + 2 \sum_{i=1}^d \left| [\nabla \mathcal{F}]_i \right| \mathbb{I}\left\{ \underbrace{\text{sgn}([\nabla \mathcal{F}]_i)}_{\mathcal{A}_i^{(\tau)}} \neq \text{sgn}([\hat{\mathbf{g}}^{(\tau)}]_i) \right\} \right), \end{aligned}$$

where $\mathbb{I}\{\cdot\}$ denotes the indicator function. Observe that the anticipated progress in the convergence hinges on the falsity of the event inside the indicator function. For brevity, we have denoted this event by $\mathcal{A}_i^{(\tau)}$. Taking the expectation conditioned on the previous iterate $\mathbf{w}^{(t)}$ yields

$$\mathbb{E}\{\Omega \mid \mathbf{w}^{(t)}\} = \sum_{\tau=0}^{T_E-1} \left(-\|\nabla \mathcal{F}\|_1 + 2 \sum_{i=1}^d \left| [\nabla \mathcal{F}]_i \right| \Pr\{\mathcal{A}_i^{(\tau)}\} \right). \quad (16)$$

Hence, if we expect the algorithm to converge, then the local gradients should at least be able to correctly guess the sign of the global gradient with high probability. The main thing now

is to bound this probability. To this end, we use the following relaxation

$$\begin{aligned} \Pr\{\mathcal{A}_i^{(\tau)}\} &\leq \Pr\left\{|\hat{\mathbf{g}}^{(\tau)}_i - [\nabla \mathcal{F}]_i| \geq |[\nabla \mathcal{F}]_i|\right\} \\ &\leq \frac{\mathbb{E}\{|\hat{\mathbf{g}}^{(\tau)}_i - [\nabla \mathcal{F}]_i|\}}{|[\nabla \mathcal{F}]_i|}, \end{aligned} \quad (17)$$

where in the second line, we have employed Markov's inequality [38]. Plugging the obtained result into (16), we get

$$\begin{aligned} \text{RHS} &\leq \sum_{\tau=0}^{T_E-1} \left(-\|\nabla \mathcal{F}\|_1 + 2 \sum_{i=1}^d \mathbb{E}\{|\hat{\mathbf{g}}^{(\tau)}_i - [\nabla \mathcal{F}]_i|\} \right) \\ &= \sum_{\tau=0}^{T_E-1} \left(-\|\nabla \mathcal{F}\|_1 \right. \\ &\quad \left. + 2 \sum_{i=1}^d \mathbb{E}\{|\hat{\mathbf{g}}^{(\tau)}_i - [\mathbf{g}^{(\tau)}_i] + [\mathbf{g}^{(\tau)}_i] - [\nabla \mathcal{F}]_i|\} \right) \\ &\leq \sum_{\tau=0}^{T_E-1} \left(-\|\nabla \mathcal{F}\|_1 + \frac{2\sigma d}{\sqrt{B}} \right. \\ &\quad \left. + 2 \sum_{i=1}^d \mathbb{E}\{|\mathbf{g}^{(\tau)}_i - [\nabla \mathcal{F}]_i|\} \right), \end{aligned} \quad (18)$$

where we have added and subtracted the true local gradient components $[\mathbf{g}^{(\tau)}_i]$ in the third line, and in the last inequality, we have used the triangle inequality along with the mini-batch gradient assumption A3.

Let us now define

$$\mathcal{I}^{(\tau)} \triangleq \sum_{i=1}^d \mathbb{E}\{|\mathbf{g}^{(\tau)}_i - [\nabla \mathcal{F}]_i|\}. \quad (19)$$

We attempt to bound $\mathcal{I}^{(\tau)}$ recursively. First, note that

$$\mathcal{I}^{(0)} = \sum_{i=1}^d \mathbb{E}\{|\mathbf{g}^{(0)}_i - [\nabla \mathcal{F}]_i|\} \quad (20a)$$

$$= \sum_{i=1}^d |[\nabla \mathcal{F}_q]_i - [\nabla \mathcal{F}]_i| = \|\nabla \mathcal{F}_q - \nabla \mathcal{F}\|_1. \quad (20b)$$

Thus, the base case is established. We next derive a recursive relation for $\mathcal{I}^{(\tau)}$

$$\begin{aligned} \mathcal{I}^{(\tau)} &= \sum_{i=1}^d \mathbb{E}\{|\mathbf{g}^{(\tau)}_i - [\nabla \mathcal{F}]_i|\} \\ &= \sum_{i=1}^d \mathbb{E}\{|\mathbf{g}^{(\tau-1)}_i - [\nabla \mathcal{F}]_i + [\mathbf{g}^{(\tau)}_i] - [\mathbf{g}^{(\tau-1)}_i]|\} \\ &\leq \sum_{i=1}^d \left(\mathbb{E}\{|\mathbf{g}^{(\tau-1)}_i - [\nabla \mathcal{F}]_i|\} \right. \\ &\quad \left. + \sum_{i=1}^d \mathbb{E}\{|\mathbf{g}^{(\tau)}_i - [\mathbf{g}^{(\tau-1)}_i]|\} \right) \\ &= \mathcal{I}^{(\tau-1)} + \mathbb{E}\{\|\nabla \mathcal{F}_q(\mathbf{v}^{(\tau)}) - \nabla \mathcal{F}_q(\mathbf{v}^{(\tau-1)})\|_1\} \\ &\leq \mathcal{I}^{(\tau-1)} + \mathbb{E}\{L\|\mathbf{v}^{(\tau)} - \mathbf{v}^{(\tau-1)}\|_\infty\} \\ &= \mathcal{I}^{(\tau-1)} + L\mu, \end{aligned}$$

where the last inequality is due to L -smoothness of \mathcal{F}_q . We have, therefore, obtained

$$\mathcal{I}^{(\tau)} \leq \mathcal{I}^{(\tau-1)} + L\mu.$$

Using this result and combining it with (20) yields

$$\begin{aligned} \mathcal{I}^{(\tau)} &\leq \mathcal{I}^{(0)} + \tau(L\mu) \\ &= \left\| \nabla \mathcal{F}_q(\mathbf{w}^{(t)}) - \nabla \mathcal{F}(\mathbf{w}^{(t)}) \right\|_1 + \tau L\mu, \end{aligned} \quad (21)$$

where we have returned to the original notation from which we temporarily deviated in (15). Plugging (21) back into (18), we get

$$\begin{aligned} \mathbb{E}\{\Omega \mid \mathbf{w}^{(t)}\} &\leq -T_E \|\nabla \mathcal{F}\|_1 + T_E \left(\frac{2\sigma d}{\sqrt{B}} \right) \\ &\quad + 2T_E \left\| \nabla \mathcal{F}_q(\mathbf{w}^{(t)}) - \nabla \mathcal{F}(\mathbf{w}^{(t)}) \right\|_1 + T_E(T_E - 1)L\mu. \end{aligned}$$

With this result, we can bound (14) after taking expectation

$$\begin{aligned} \mathbb{E}\left\{ -\mu \sum_{q=1}^Q \frac{D_q}{N} \sum_{\tau=0}^{T_E-1} \left\langle \nabla \mathcal{F}(\mathbf{w}^{(t)}), \text{sgn}(\hat{\mathbf{g}}_q^{(t,\tau)}) \right\rangle \right\} \\ \leq \mu \left(-T_E \|\nabla \mathcal{F}\|_1 + \frac{2\sigma d T_E}{\sqrt{B}} + 2T_E \zeta + T_E(T_E - 1)L\mu \right). \end{aligned}$$

Combining this with the bounded second term, we get

$$\frac{\mathbb{E}\{\mathcal{F}(\mathbf{w}^{(t+1)}) - \mathcal{F}(\mathbf{w}^{(t)}) \mid \mathbf{w}^{(t)}\}}{\mu T_E} \leq -\|\nabla \mathcal{F}(\mathbf{w}^{(t)})\|_1 + C,$$

where

$$C = 2\zeta + \frac{2\sigma d}{\sqrt{B}} + \left(\frac{3T_E}{2} - 1 \right) L\mu.$$

Finally, we extend the expectation over the randomness in the process, apply a telescoping sum over the iterations, and rearrange to achieve the averaged performance bound

$$\frac{1}{T_G} \sum_{t=0}^{T_G-1} \mathbb{E}\{\|\nabla \mathcal{F}(\mathbf{w}^{(t)})\|_1\} \leq \frac{\mathcal{F}(\mathbf{w}^{(0)}) - \mathcal{F}^*}{\mu T_G T_E} + C.$$

□

Remark 1: The first term on the right-hand side of (9) tends to zero as the number of global aggregation rounds T_G increases. By tuning μ and B , the components of C can also be reduced, except for the 2ζ term, which stems from the enforced non-IID data distribution across edge servers. The following corollary highlights this.

Corollary 2. *Assuming an IID inter-edge data distribution, so that, in the large-network limit, $\zeta \rightarrow 0$, and choosing $\mu = 1/\sqrt{T_G}$ and $B = T_G$, we obtain a worst-case sublinear convergence rate of $\mathcal{O}(1/\sqrt{T_G})$ for HierSignSGD:*

$$\frac{1}{T_G} \sum_{t=0}^{T_G-1} \mathbb{E}\{\|\nabla \mathcal{F}(\mathbf{w}^{(t)})\|_1\} \leq \frac{1}{\sqrt{T_G}} \left(\frac{\mathcal{F}(\mathbf{w}^{(0)}) - \mathcal{F}^*}{T_E} + \tilde{C} \right) \quad (22)$$

where

$$\tilde{C} = 2\sigma d + \left(\frac{3T_E}{2} - 1 \right) L.$$

From Corollary 2, it follows that as $T_G \rightarrow \infty$, we get

$$\min_{0 \leq t \leq T_G-1} \mathbb{E}\left\{\|\nabla \mathcal{F}(\mathbf{w}^{(t)})\|_1\right\} \rightarrow 0, \quad (23)$$

indicating that the algorithm produces a sequence whose *best iterate* converges on average to a stationary point.

Remark 2: The upper bound derived in Theorem 1 depends nonmonotonically on T_E , implying that an optimal value of T_E exists that minimizes the bound. This indicates that, in practice, the number of edge-device communication rounds may have a performance *sweet spot*. We shall investigate this phenomenon in our simulations under IID and non-IID data partitioning schemes across edge servers.

Extending the obtained result to the majority-vote setting, where each cluster consists of M devices, we have the following theorem:

Theorem 3. *Under the assumptions of Theorem 1, but with each server now handling M devices, the proposed algorithm attains the same convergence bound as in Theorem 1.*

Proof. See Appendix A. \square

Remark 3: While Theorem 3 and its proof in Appendix A show that majority voting over M signs can only be beneficial, it is also important to investigate the effect M has on ζ . As we show in Appendix C, in the case of inter-edge IID sample distribution, we have $\zeta = \mathcal{O}(M^{-1/2})$. This result demonstrates that the impact of ζ decreases as additional intra-cluster devices are incorporated, a point briefly invoked in Corollary 2 as part of the assumptions. In the non-IID case, though, enlarging M cannot circumvent the intrinsic inter-cluster heterogeneity present in non-IID data environments. In this case, each cluster possesses its own underlying mean gradient, determined by its local data distribution. Increasing M inside a cluster reduces only the sampling noise in the empirical cluster gradient. It does *not* eliminate the inherent mismatch between the true cluster-level means. Hence, even as $M \rightarrow \infty$, the heterogeneity measure ζ converges to a value determined by the distributional differences across clusters.

C. Extension to Downlink Quantization

When further reducing communication costs over the channel is necessary, we may employ a compressed broadcast of the global model. This approach also renders the communication between edge servers and devices fully binary-compatible, an attractive feature in systems where devices operate with very simple modulation-demodulation capabilities. To this end, HierSignSGD needs a modification in the step 2 of Section III-A. Each edge server now quantizes the difference between the true model and the previously obtained device model as $\mathcal{Z}(\mathbf{w}^{(t)} - \mathbf{v}_q^{(t-1,0)})$, where $\mathcal{Z}(\cdot)$ is the quantization operator, and broadcasts it to its associated devices. The devices subsequently form the following estimate of the model

$$\mathbf{v}_q^{(t,0)} = \mathbf{v}_q^{(t-1,0)} + \mathcal{Z}(\mathbf{w}^{(t)} - \mathbf{v}_q^{(t-1,0)}), \quad (24)$$

where we take $\mathbf{v}_q^{(0,0)} = \mathbf{w}^{(0)}$. Note that quantizing the model difference reduces communication cost of model broadcast,

since the updates shrink in magnitude as the model approaches a stationary point. A typical stochastic quantizer to employ is one that possesses the following properties [17]:

$$\begin{aligned} \mathbb{E}_{\mathcal{Z}}\{\mathcal{Z}(\mathbf{w}) \mid \mathbf{w}\} &= \mathbf{w}, \\ \mathbb{E}_{\mathcal{Z}}\{\|\mathcal{Z}(\mathbf{w}) - \mathbf{w}\|_2^2 \mid \mathbf{w}\} &\leq \psi^2 \|\mathbf{w}\|_2^2 \quad (\forall \mathbf{w} \in \mathbb{R}^d), \end{aligned} \quad (25)$$

where the first property indicates that $\mathcal{Z}(\cdot)$ is unbiased, while the second one bounds its variance. In Appendix B, we establish a corresponding convergence bound for the extended HierSignSGD; the resulting expression is presented below.

Theorem 4. *With downlink quantization applied to the model difference during edge broadcast, and under the assumptions of Theorem 1, the modified HierSignSGD attains the following error bound:*

$$\frac{1}{T_G} \sum_{t=0}^{T_G-1} \mathbb{E}\left\{\|\nabla \mathcal{F}(\mathbf{w}^{(t)})\|_1\right\} \leq \frac{\mathcal{F}(\mathbf{w}^{(0)}) - \mathcal{F}^*}{\mu T_G T_E} + C_{\mathcal{Z}}, \quad (26)$$

where

$$C_{\mathcal{Z}} = C + \psi \sqrt{d} \left(3 + \frac{\psi \sqrt{d}}{2} \right) L \mu T_E.$$

Proof. See Appendix B. \square

Remark 4: Although the additional error term in (26) introduced by quantization can negatively affect convergence, an appropriate choice of the step-size μ , similar to that in Corollary 2, can effectively mitigate its effect.

IV. SIMULATIONS

To evaluate the performance of HierSignSGD, we conduct a series of experiments on the EMNIST-digits dataset¹, a widely used benchmark for large-scale and distributed learning. Additionally, we report classification accuracy results on the more challenging Fashion-MNIST dataset² to more rigorously examine performance under a deeper and more complex learning model. However, the remainder of the simulations are conducted only on the EMNIST digits, as its simple learning model allows us to better isolate and understand the effects of the key parameters in the SignSGD update rule without confounding them with the complexity of a deeper model.

A. Setup

The learning model used for the EMNIST-digits experiments is a fully connected neural network with a single hidden layer containing 30 units, for which training is performed using the cross-entropy loss applied to the output logits. For the Fashion-MNIST experiments, we employ a convolutional neural network consisting of two 3×3 convolutional layers with 32 and 64 channels, respectively. Each convolution is followed by a ReLU activation and a 2×2 max-pooling operation. The resulting feature map is flattened and passed through

¹EMNIST is a benchmark dataset derived from the NIST Special Database 19 [39]. It augments MNIST by incorporating handwritten digits and letters, thereby providing a richer and more diverse character-classification task.

²A clothing-image dataset, designed as a more challenging drop-in replacement for MNIST for benchmarking learning algorithms [40].

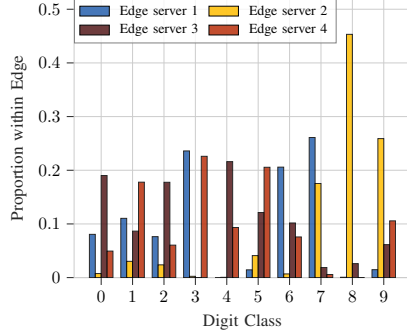


Fig. 2. EMNIST-digits proportions per edge server under dirichlet non-IID partition ($\alpha = 0.3$)

a fully connected layer with 128 hidden units, followed by a 10-way output layer.

Unless stated otherwise, simulations in our two-tier HFL setup use $Q = 4$ edge servers and $M = 5$ devices per edge, totaling 20 participating devices. Both IID and non-IID scenarios are considered. In the non-IID setting, statistical heterogeneity across edge servers is induced through a symmetric Dirichlet distribution, while keeping the devices within each edge IID to isolate the effect of edge-level skew. For each class m , a probability vector is sampled according to

$$\mathbf{p}_m \sim \text{Dirichlet}(\alpha \mathbf{1}_Q),$$

where α controls the concentration parameter. Each entry $[\mathbf{p}_m]_q$ represents the fraction of class- m samples assigned to edge server q . Smaller α values yield imbalanced (non-IID) device label distributions, while larger α values produce more uniform (IID-like) partitions. We set $\alpha = 0.3$ for our case. Fig. 2 shows the distribution of digit labels across edge servers, clearly illustrating that the data partitioning is fairly heterogeneous.

B. Learning Accuracy

As a first scenario, we examine how HierSignSGD compares to its SGD-based counterpart, which we denote by HierSGD for consistency. In HierSGD, devices transmit their full gradients to the edge server, which computes a weighted average of these gradients before performing a standard gradient descent update. We tune the hyperparameters of both methods as carefully as possible, guided by empirical experimentation and by choices commonly favored in the literature. In our experiments, we found that tuning the batch-size had a far greater impact on the convergence of HierSignSGD than any other hyperparameter. The results for both datasets depicted in Fig. 3 show that, in the IID case, HierSignSGD attains higher test accuracy more efficiently. In the non-IID case, however, HierSGD initially performs better, with HierSignSGD closing the gap after about 30 global rounds. Beyond accuracy, we also examine the communication efficiency of the two methods. Assuming that standard SGD transmits 32 bits per dimension and that device-edge communication occurs every 10 ms, our results show that HierSignSGD is able to achieve substantially lower bit rates (see Table III).

TABLE III
BIT-RATE COMPARISON

Dataset	d	HierSignSGD Bit Rate	HierSGD Bit Rate
EMNIST	23,860	2.39 Mbps	76.35 Mbps
Fashion-MNIST	421,642	42.16 Mbps	1.35 Gbps

The observation that SignSGD might outperform conventional SGD in training neural networks on handwritten digit datasets is somewhat expected. The improved performance of SignSGD can be attributed to the structure of the gradient noise, which depends on the statistical properties of the dataset. When the noise exhibits large variance in magnitude or heavy-tailed behavior, conditions under which the gradient direction remains more reliable than its magnitude, the sign operator provides a more robust update than standard SGD. Under such noise characteristics, which have been observed in fully connected neural networks trained on the MNIST dataset [41], [42], SignSGD can outperform full-precision SGD because it relies solely on the directional information of the gradient, thereby suppressing magnitude-induced fluctuations. Although no heavy-tail analysis of EMNIST has been reported, it is reasonable to expect similar gradient-noise characteristics given its structural similarity to MNIST. However, this intuition holds primarily under IID data partitioning. When the data are distributed heterogeneously across edge servers, the statistical properties of the local gradients can change significantly, which may alter the behavior of both SGD and SignSGD-based algorithms. Potential heavy-tailed behavior in Fashion-MNIST offers a similar explanation.

C. Effect of T_E

For the second scenario, we aim to assess how the number of edge-device communication rounds influences overall performance. As discussed in Remark 2, the choice of the design parameter T_E can significantly influence the algorithm's performance. We therefore investigate its effect empirically. As shown in Fig. 4, in the IID setting increasing T_E generally accelerates training. This is expected, since all edge servers operate on statistically similar data, and additional local steps effectively mimic more frequent global aggregations. In contrast, in the non-IID setting we observe that beyond a certain point, increasing T_E degrades performance. The results suggest that $T_E \approx 30$ strikes a good balance. When local training is carried out for too long without the smoothing effect of global aggregation, each edge server drifts toward the minimizer of its local objective; under data heterogeneity, these local minima can deviate substantially from the minimizer of the global objective.

D. Cluster Reconfiguration

In this part, we investigate the effect of different device groupings on the training loss. Specifically, we vary the number of devices per edge M and the number of edge servers Q while keeping the total number of participating devices fixed at $M \times Q = 48$. We focus exclusively on the IID setting, as the non-IID case introduces substantial stochasticity and

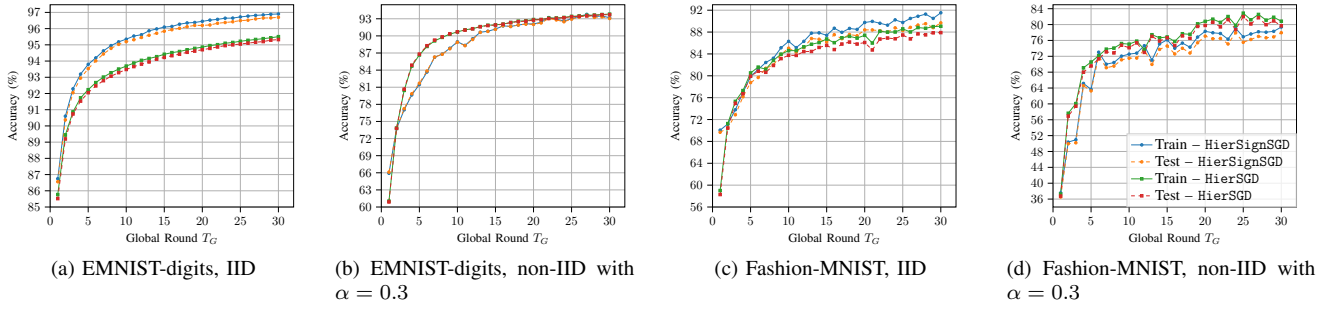
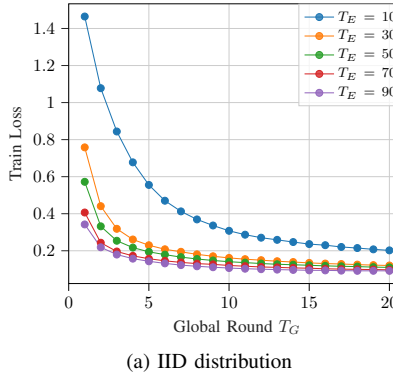
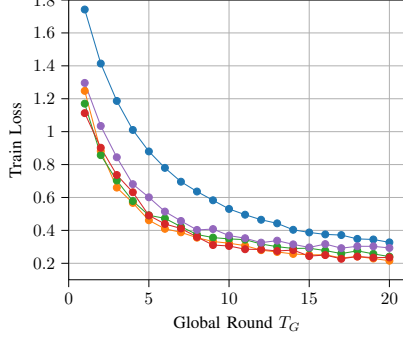


Fig. 3. Test accuracy comparison between HierSignSGD and HierSGD on EMNIST-digits and Fashion-MNIST. We use a batch-size of $B = 400$. Step-size μ : EMNIST—1 (HierSGD), 5×10^{-3} (HierSignSGD); Fashion-MNIST—0.1 (HierSGD), 7×10^{-4} (HierSignSGD).



(a) IID distribution



(b) Non-IID distribution with $\alpha = 0.3$

Fig. 4. Effect of T_E on global training loss for HierSignSGD.

the behavior of majority-vote aggregation under heterogeneous device distributions is not trivial to interpret. Intuitively, with a larger number of edges, the global averaging step can better mitigate the effects of statistical variability by reducing edge-level noise and stabilizing the updates across the hierarchy. However, increasing Q necessarily reduces M , which weakens the reliability of the majority-vote mechanism at each edge. Moreover, as noted in *Remark 3*, increasing M can help mitigate gradient dissimilarity. On the other hand, from a practical point of view, selecting too few edge servers is also undesirable. If Q is too small, the system loses the main architectural benefit of a hierarchical implementation: scalability. Thus, we are encouraged to find a compromise as the optimal clustering lies somewhere in between. The plot in Fig. 5, showing the average training loss over five random device groupings for each (Q, M) pair, appears to validate our intuition. Observe that neither extreme case, $Q = 1$ nor $Q = 48$, yields optimal performance, demonstrating that we

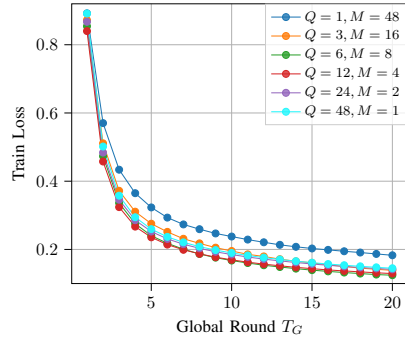


Fig. 5. Training sensitivity to different clusterings of $M \times Q = 48$ IID devices.

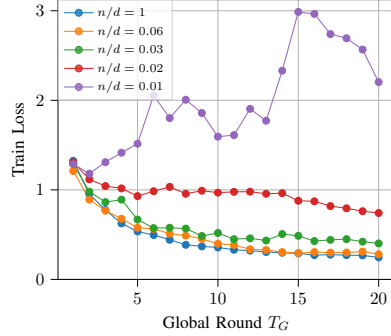


Fig. 6. Plotting global train loss of HierSignSGD with downlink random sparsification of the global model (non-IID).

do in fact benefit from a *balanced* HFL design.

E. Effect of Downlink Quantization

In the final part of our analysis, we examine the impact of downlink quantization on performance. We utilize a random sparsification scheme with n active components, given by

$$\mathcal{Z}(\mathbf{x}) = \frac{d}{n} (\mathbf{e} \odot \mathbf{x}), \quad (27)$$

where \mathbf{e} is a random binary vector with n nonzero entries, and \odot denotes the component-wise product. It can be easily shown that $\mathcal{Z}(\mathbf{x})$ satisfies (25). We vary the sparsification level and examine its effect on convergence under a non-IID distribution. As shown in Fig. 6, even with aggressive quantization, down to $n/d = 0.06$, the performance remains largely unaffected.

However, beyond a certain point the degradation becomes significant, with a clear breaking point around $n/d \approx 0.01$.

V. CONCLUSION

In this paper, we presented HierSignSGD, a highly communication-efficient algorithm for the problem of HFL. By combining clustering, sign-based gradient transmission, majority-vote aggregation at the edge, and quantized downlink broadcasts, the method substantially reduces communication overhead while retaining effective learning performance. We established the first convergence analysis for hierarchical SignSGD in nonconvex settings and quantified the impact of biased compression, aggregation intervals, and inter-cluster heterogeneity. Experiments under IID and non-IID partitions confirmed the theoretical insights, showing competitive accuracy relative to SGD-based methods and robustness to aggressive sparsification for downlink broadcast. These results provide a foundation for highly communication-efficient HFL and suggest several future directions, including extensions to deeper hierarchies, adaptive clustering, and enhanced sign-based optimization schemes.

APPENDIX A MAJORITY-VOTE ERROR ANALYSIS

In this section, we generalize the results of Theorem 1 to the case in which each edge server manages a cluster of M devices. We reiterate that the convergence of HierSignSGD in the case of a single-device edge server primarily hinges on the probability of an incorrect sign estimate remaining bounded:

$$P_e = \Pr \left\{ \operatorname{sgn}([\nabla \mathcal{F}]_i) \neq \operatorname{sgn}([\hat{\mathbf{g}}^{(\tau)}]_i) \right\}, \quad (28)$$

where we have denoted this probability by P_e . We also established a bound for P_e via (17). Essentially, this bound was obtained through the following procedure

$$\begin{aligned} P_e &\leq \frac{\mathbb{E} \left\{ |[\hat{\mathbf{g}}^{(\tau)}]_i - [\nabla \mathcal{F}]_i| \right\}}{|[\nabla \mathcal{F}]_i|} \\ &= \frac{\mathbb{E} \left\{ |[\hat{\mathbf{g}}^{(\tau)}]_i - [\mathbf{g}^{(\tau)}]_i| + |[\mathbf{g}^{(\tau)}]_i - [\nabla \mathcal{F}]_i| \right\}}{|[\nabla \mathcal{F}]_i|} \\ &\leq \frac{\nu}{|[\nabla \mathcal{F}]_i|} + \frac{\mathbb{E} \{ |\beta| \}}{|[\nabla \mathcal{F}]_i|} =: \psi, \end{aligned}$$

where here ψ denotes the bound on P_e , $\beta = [\mathbf{g}^{(\tau)}]_i - [\nabla \mathcal{F}]_i$, and $\nu^2 = \mathbb{E} \left\{ |[\hat{\mathbf{g}}^{(\tau)}]_i - [\mathbf{g}^{(\tau)}]_i|^2 \right\}$.

When introducing the majority-vote mechanism, however, the new probability of error becomes

$$P_e^{(M)} = \Pr \left\{ \operatorname{sgn}([\nabla \mathcal{F}]_i) \neq \operatorname{sgn} \left(\sum_{k \in \mathcal{V}^q} \operatorname{sgn}([\hat{\mathbf{g}}_k^{(\tau)}]_i) \right) \right\}.$$

Similar to [18], we argue that this probability is bounded by the same threshold as in (28). In other words, if $P_e \leq \psi$, then $P_e^{(M)} \leq \psi$. There are two cases to consider: when $\psi \geq 1$, the inequality $P_e^{(M)} \leq \psi$ is immediate; when $\psi < 1$, more careful examination is required. Without loss of generality assume that $\operatorname{sgn}([\nabla \mathcal{F}]_i) = -1$. Then,

$$P_e = \Pr \left\{ [\hat{\mathbf{g}}^{(\tau)}]_i > 0 \right\} = \Pr \left\{ [\hat{\mathbf{g}}^{(\tau)}]_i - \overline{[\mathbf{g}^{(\tau)}]_i} > -\overline{[\mathbf{g}^{(\tau)}]_i} \right\}.$$

Now, note that

$$\begin{aligned} -\overline{[\mathbf{g}^{(\tau)}]_i} &= -\mathbb{E}\{\beta\} - [\nabla \mathcal{F}]_i = -\mathbb{E}\{\beta\} + |[\nabla \mathcal{F}]_i| \\ &\geq -\mathbb{E}\{|\beta|\} + |[\nabla \mathcal{F}]_i| \geq \nu > 0, \end{aligned}$$

where the last inequality is simply due to $\psi \leq 1$. Hence, $-\overline{[\mathbf{g}^{(\tau)}]_i} \geq 0$ and we can use Cantelli's inequality [38] to obtain a tight one-sided tail bound:

$$\begin{aligned} P_e &= \Pr \left\{ [\hat{\mathbf{g}}^{(\tau)}]_i - \overline{[\mathbf{g}^{(\tau)}]_i} > -\overline{[\mathbf{g}^{(\tau)}]_i} \right\} \\ &\leq \frac{\nu^2}{\nu^2 + \overline{[\mathbf{g}^{(\tau)}]_i}^2} \leq \frac{\nu^2}{\nu^2 + \nu^2} = \frac{1}{2}. \end{aligned}$$

Therefore, we have obtained $P_e < 1/2$ when $\psi \leq 1$ (the same analysis holds when $[\nabla \mathcal{F}]_i$ is positive). As we shall see, this result is crucial for the final step of the argument.

We now draw an analogy to our problem by considering a fundamental channel coding scenario. Suppose a single information bit (0 or 1) is repeatedly transmitted over a noisy channel. In this setting, the maximum a posteriori (MAP) detector, optimal for minimizing the probability of detection error [43], reduces to a simple majority-vote rule applied to the received samples as the following illustrates. Let b be the bit sent, repeated M times. The channel flips each bit with probability P_e , independently (owing to the IID assumption across the device cluster). Let r be what we receive, and let n be the number of 1's in r .

- If $b = 0$ was sent, the number of errors equals n :

$$\Pr\{r \mid b = 0\} = P_e^n (1 - P_e)^{M-n}.$$

- If $b = 1$ was sent, the number of errors equals $M - n$:

$$\Pr\{r \mid b = 1\} = P_e^{M-n} (1 - P_e)^n.$$

With an equiprobable prior on b , the MAP detector chooses the b with larger likelihood:

$$\frac{\Pr\{r \mid b = 1\}}{\Pr\{r \mid b = 0\}} = \left(\frac{1 - P_e}{P_e} \right)^{2n - M}.$$

Since we have established that $P_e < 1/2$, the ratio is > 1 exactly when $n > M/2$. This is precisely *majority-vote*. For the case $n = M/2$, the likelihood ratio equals 1, meaning that the MAP rule has no preference between 0 and 1 and may choose either value, for example by random tie-breaking. We reiterate that MAP is optimal, meaning that no alternative decoding rule can achieve a smaller probability of error than majority-vote, including the crude decoder that examines only the first received bit and outputs it. In other words, $P_e^{(M)} < P_e$, and the bound in Theorem 1, which is looser than ψ , also holds for the majority-vote case.

APPENDIX B BOUND DERIVATION UNDER DOWNLINK QUANTIZATION

To begin our analysis, the key observation is that the update for $\mathbf{w}^{(t+1)}$ in (10) now takes the form

$$\mathbf{w}^{(t+1)} = \mathbf{v}_q^{(t,0)} - \mu \sum_{q=1}^Q \sum_{\tau=0}^{T_E-1} \frac{D_q}{N} \operatorname{sgn}(\hat{\mathbf{g}}_q^{(t,\tau)}) \quad (29a)$$

$$= \mathbf{v}_q^{(t-1,0)} + \mathcal{Z}(\mathbf{w}^{(t)} - \mathbf{v}_q^{(t-1,0)}) + \boldsymbol{\chi}^{(t)}, \quad (29b)$$

where we have set

$$\chi^{(t)} \triangleq -\mu \sum_{q=1}^Q \sum_{\tau=0}^{T_E-1} \frac{D_q}{N} \operatorname{sgn}(\hat{g}_q^{(t, \tau)}),$$

for brevity. Adding and subtracting $\mathbf{w}^{(t)}$ on the RHS of (29b), we obtain a more interpretable expression for the global update

$$\mathbf{w}^{(t+1)} = \mathbf{w}^{(t)} + \chi^{(t)} + \mathcal{Z}(\Delta^{(t)}) - \Delta^{(t)}, \quad (30)$$

where $\Delta^{(t)} \triangleq \mathbf{w}^{(t)} - \mathbf{v}_q^{(t-1, 0)}$ denotes the model difference. Notice that (30) resembles (10), except that it now includes the quantization error $\epsilon^{(t)} \triangleq \mathcal{Z}(\Delta^{(t)}) - \Delta^{(t)}$. Using (30), we now derive the upper bounds for the two terms in (11). For the second term, we have

$$\begin{aligned} \frac{L}{2} \left\| \mathbf{w}^{(t+1)} - \mathbf{w}^{(t)} \right\|_{\infty}^2 &= \frac{L}{2} \left\| \chi^{(t)} + \epsilon^{(t)} \right\|_{\infty}^2 \\ &\leq \frac{L}{2} \left(\mu T_E + \|\epsilon^{(t)}\|_{\infty} \right)^2 \leq \frac{L}{2} \left(\mu T_E + \|\epsilon^{(t)}\|_2 \right)^2, \end{aligned}$$

where we have used norm inequalities and result of (13). Taking the expectation and applying the quantizer's variance bound yield

$$\begin{aligned} \frac{L}{2} \mathbb{E}_{\mathcal{Z}} \left\{ \left\| \mathbf{w}^{(t+1)} - \mathbf{w}^{(t)} \right\|_{\infty}^2 \right\} &\leq \frac{L}{2} \left(\mu T_E + \mathbb{E}_{\mathcal{Z}} \{ \|\epsilon^{(t)}\|_2 \} \right)^2 \\ &\leq \frac{L}{2} \left(\mu T_E + \mathbb{E}_{\mathcal{Z}} \{ \psi \|\Delta^{(t)}\|_2 \} \right)^2 = \frac{L}{2} \left(\mu T_E + \psi \|\chi^{(t-1)}\|_2 \right)^2 \\ &\leq \frac{L}{2} \left(\mu T_E + \psi \mu T_E \sqrt{d} \right)^2 = \frac{L}{2} (\mu T_E)^2 (1 + \psi \sqrt{d})^2. \quad (31) \end{aligned}$$

Next, we bound the first term of (11)

$$\langle \nabla \mathcal{F}(\mathbf{w}^{(t)}), \chi^{(t)} + \epsilon^{(t)} \rangle,$$

but to avoid repeating the entire procedure, we point out only the necessary modifications. First, observe that upon applying the expectation $\mathbb{E}_{\mathcal{Z}}$, the inner product $\langle \nabla \mathcal{F}(\mathbf{w}^{(t)}), \epsilon^{(t)} \rangle$ will disappear, owing to the unbiased property of $\mathcal{Z}(\cdot)$. For $\langle \nabla \mathcal{F}(\mathbf{w}^{(t)}), \chi^{(t)} \rangle$, the only step that we should redo is when establishing the base case $\mathcal{I}^{(0)}$ for our recursion (see (20a) and (15)):

$$\begin{aligned} \mathcal{I}^{(0)} &= \sum_{i=1}^d \mathbb{E} \left\{ |[\mathbf{g}^{(0)}]_i - [\nabla \mathcal{F}]_i| \right\} \\ &= \sum_{i=1}^d \mathbb{E} \left\{ |[\nabla \mathcal{F}_q(\mathbf{v}_q^{(t, 0)})]_i - [\nabla \mathcal{F}]_i| \right\} \\ &= \sum_{i=1}^d \mathbb{E} \left\{ |[\nabla \mathcal{F}_q(\mathbf{v}_q^{(t, 0)})]_i - [\nabla \mathcal{F}_q]_i + [\nabla \mathcal{F}_q]_i - [\nabla \mathcal{F}]_i| \right\} \\ &\leq \mathbb{E} \left\{ \|\nabla \mathcal{F}_q(\mathbf{v}_q^{(t, 0)}) - \nabla \mathcal{F}_q(\mathbf{w}^{(t)})\|_1 \right\} + \|\nabla \mathcal{F}_q - \nabla \mathcal{F}\|_1 \\ &\leq \mathbb{E} \left\{ L \|\mathbf{v}_q^{(t, 0)} - \mathbf{w}^{(t)}\|_{\infty} \right\} + \|\nabla \mathcal{F}_q - \nabla \mathcal{F}\|_1 \\ &= \mathbb{E} \left\{ L \|\epsilon^{(t)}\|_{\infty} \right\} + \|\nabla \mathcal{F}_q - \nabla \mathcal{F}\|_1 \\ &\leq L (\psi \mu T_E \sqrt{d}) + \|\nabla \mathcal{F}_q - \nabla \mathcal{F}\|_1, \end{aligned}$$

where we have used the L -smoothness of \mathcal{F}_q (assumption A2) and the bound for $\mathbb{E} \{ \|\epsilon^{(t)}\|_{\infty} \}$ derived in (31). Incorporating these modifications into our convergence analysis, we arrive at Theorem 4.

APPENDIX C SCALING BEHAVIOR OF ζ IN THE IID SETTING

Let us define

$$\tilde{\zeta}(M, \mathbf{w}) \triangleq \sum_{q=1}^Q \frac{D_q}{N} \|\nabla \mathcal{F}_q(\mathbf{w}) - \nabla \mathcal{F}(\mathbf{w})\|_1.$$

Assuming the fully IID model across all devices, we have for the device gradients

$$\mathbb{E}_{\xi \sim \mathcal{D}} \{ \nabla f_{qk}(\mathbf{w}) \} =: \nabla f(\mathbf{w}),$$

with their respective covariance matrix $\mathbf{Cov}(\mathbf{w})$. Using the triangle inequality yields

$$\begin{aligned} \|\nabla \mathcal{F}_q(\mathbf{w}) - \nabla \mathcal{F}(\mathbf{w})\|_1 &\leq \|\nabla \mathcal{F}_q(\mathbf{w}) - \nabla f(\mathbf{w})\|_1 + \|\nabla \mathcal{F}(\mathbf{w}) - \nabla f(\mathbf{w})\|_1, \end{aligned}$$

and

$$\begin{aligned} \|\nabla \mathcal{F}(\mathbf{w}) - \nabla f(\mathbf{w})\|_1 &= \left\| \sum_{q=1}^Q \frac{D_q}{N} (\nabla \mathcal{F}_q(\mathbf{w}) - \nabla f(\mathbf{w})) \right\|_1 \\ &\leq \sum_{q=1}^Q \frac{D_q}{N} \|\nabla \mathcal{F}_q(\mathbf{w}) - \nabla f(\mathbf{w})\|_1. \end{aligned}$$

Therefore,

$$\tilde{\zeta}(M, \mathbf{w}) \leq 2 \sum_{q=1}^Q \frac{D_q}{N} \|\nabla \mathcal{F}_q(\mathbf{w}) - \nabla f(\mathbf{w})\|_1.$$

Taking expectation and using statistical symmetry of the clusters,

$$\mathbb{E}_{\xi \sim \mathcal{D}} \{ \tilde{\zeta}(M, \mathbf{w}) \} \leq 2 \mathbb{E} \{ \|\nabla \mathcal{F}_1(\mathbf{w}) - \nabla f(\mathbf{w})\|_1 \}.$$

Employing norm and Jensen's inequalities, we get

$$\begin{aligned} \mathbb{E} \{ \|\nabla \mathcal{F}_1(\mathbf{w}) - \nabla f(\mathbf{w})\|_1 \} &\leq \sqrt{d} \mathbb{E} \{ \|\nabla \mathcal{F}_1(\mathbf{w}) - \nabla f(\mathbf{w})\|_2 \} \\ &\leq \frac{\sqrt{d \times \operatorname{trace}(\mathbf{Cov}(\mathbf{w}))}}{\sqrt{M}}. \end{aligned}$$

Combining the estimates,

$$\mathbb{E}_{\xi \sim \mathcal{D}} \{ \tilde{\zeta}(M, \mathbf{w}) \} \leq 2 \frac{\sqrt{d \times \operatorname{trace}(\mathbf{Cov}(\mathbf{w}))}}{\sqrt{M}}.$$

Now, we can set the heterogeneity parameter ζ to be

$$\zeta = \sup_{\mathbf{w}} \mathbb{E}_{\xi \sim \mathcal{D}} \{ \tilde{\zeta}(M, \mathbf{w}) \},$$

where the notation \sup denotes supremum, and if the covariance trace is uniformly bounded,

$$\sup_{\mathbf{w}} \operatorname{trace}(\mathbf{Cov}(\mathbf{w})) < \infty,$$

then,

$$\zeta = \mathcal{O}(M^{-1/2}).$$

REFERENCES

[1] B. McMahan, E. Moore, D. Ramage, S. Hampson, and B. A. y Arcas, "Communication-efficient learning of deep networks from decentralized data," in *Artificial intelligence and statistics*. PMLR, 2017, pp. 1273–1282.

[2] A. Reisizadeh, A. Mokhtari, H. Hassani, A. Jadbabaie, and R. Pedarsani, "FedPAQ: A communication-efficient federated learning method with periodic averaging and quantization," in *International conference on artificial intelligence and statistics*. PMLR, 2020, pp. 2021–2031.

[3] A. Reisizadeh, I. Tziotis, H. Hassani, A. Mokhtari, and R. Pedarsani, "Straggler-resilient federated learning: Leveraging the interplay between statistical accuracy and system heterogeneity," *IEEE Journal on Selected Areas in Information Theory*, vol. 3, no. 2, pp. 197–205, 2022.

[4] W. Shi, S. Zhou, Z. Niu, M. Jiang, and L. Geng, "Joint device scheduling and resource allocation for latency constrained wireless federated learning," *IEEE Transactions on Wireless Communications*, vol. 20, no. 1, pp. 453–467, 2020.

[5] D. Jhunjhunwala, A. Gadhikar, G. Joshi, and Y. C. Eldar, "Adaptive quantization of model updates for communication-efficient federated learning," in *IEEE International Conference on Acoustics, Speech and Signal Processing (ICASSP)*, 2021, pp. 3110–3114.

[6] T. Castiglia, A. Das, and S. Patterson, "Multi-level local SGD: Distributed SGD for heterogeneous hierarchical networks," in *International Conference on Learning Representations*, 2021.

[7] L. Liu, J. Zhang, S. Song, and K. B. Letaief, "Hierarchical federated learning with quantization: Convergence analysis and system design," *IEEE Transactions on Wireless Communications*, vol. 22, no. 1, pp. 2–18, 2022.

[8] S. M. Azimi-Abarghouyi, N. Bastianello, K. H. Johansson, and V. Fodor, "Hierarchical federated ADMM," *IEEE Networking Letters*, 2025.

[9] S. M. Azimi-Abarghouyi and V. Fodor, "A hierarchical federated learning approach for the Internet of Things," *arXiv preprint arXiv:2403.01540*, 2024.

[10] K. Bonawitz, D. Huba, and et al., "Towards federated learning at scale: System design," in *MLSYS*, 2019.

[11] S. Wang, T. Tuor, and et al., "Adaptive federated learning in resource constrained edge computing," *IEEE Journal on Selected Areas in Communications*, 2019.

[12] H. Yang, X. Liu, and T. Quek, "Federated learning via over-the-air computation," *IEEE Transactions on Wireless Communications*, 2020.

[13] G. Zhu, Y. Liu, and et al., "Broadband analog aggregation for low-latency federated edge learning," *IEEE Transactions on Wireless Communications*, 2020.

[14] J. Fang, J. Li, and et al., "Energy-efficient distributed sensing in wireless networks," *IEEE Signal Processing Magazine*, 2020.

[15] X. Jiang and H. Zhu, "On the convergence of hierarchical federated learning with partial worker participation," in *The 40th Conference on Uncertainty in Artificial Intelligence*, 2024.

[16] X. Liu, S. Wang, Y. Deng, and A. Nallanathan, "Adaptive federated pruning in hierarchical wireless networks," *IEEE Transactions on Wireless Communications*, vol. 23, no. 6, pp. 5985–5999, 2023.

[17] D. Alistarh, D. Grubic, J. Li, R. Tomioka, and M. Vojnovic, "QSGD: Communication-efficient SGD via gradient quantization and encoding," *Advances in neural information processing systems*, vol. 30, 2017.

[18] J. Bernstein, Y.-X. Wang, K. Azizzadenesheli, and A. Anandkumar, "SignSGD: Compressed optimisation for non-convex problems," in *International conference on machine learning*. PMLR, 2018, pp. 560–569.

[19] S. P. Karimireddy, Q. Rebjock, S. Stich, and M. Jaggi, "Error feedback fixes SignSGD and other gradient compression schemes," in *International conference on machine learning*. PMLR, 2019, pp. 3252–3261.

[20] M. Safaryan and P. Richtárik, "Stochastic sign descent methods: New algorithms and better theory," in *International Conference on Machine Learning*. PMLR, 2021, pp. 9224–9234.

[21] W. Jiang, S. Yang, W. Yang, and L. Zhang, "Efficient sign-based optimization: Accelerating convergence via variance reduction," *Advances in Neural Information Processing Systems*, vol. 37, pp. 33 891–33 932, 2024.

[22] E. Chzhen and S. Schechtman, "SignSVRG: fixing SignSGD via variance reduction," *arXiv preprint arXiv:2305.13187*, 2023.

[23] T. Sun, Q. Wang, D. Li, and B. Wang, "Momentum ensures convergence of SignSGD under weaker assumptions," in *International Conference on Machine Learning*. PMLR, 2023, pp. 33 077–33 099.

[24] D. Wang, M. Giordani, M.-S. Alouini, and M. Zorzi, "The potential of multilayered hierarchical nonterrestrial networks for 6G: A comparative analysis among networking architectures," *IEEE Vehicular Technology Magazine*, vol. 16, no. 3, pp. 99–107, 2021.

[25] H. S. Dhillon, R. K. Ganti, F. Baccelli, and J. G. Andrews, "Modeling and analysis of K-tier downlink heterogeneous cellular networks," *IEEE Journal on Selected Areas in Communications*, vol. 30, no. 3, pp. 550–560, 2012.

[26] S. M. Azimi-Abarghouyi and C. Fischione, "Multi-layer hierarchical federated learning with quantization," *arXiv preprint arXiv:2505.08145*, 2025.

[27] O. Aygün, M. Kazemi, D. Gündüz, and T. M. Duman, "Over-the-air federated edge learning with hierarchical clustering," *IEEE Transactions on Wireless Communications*, 2024.

[28] S. M. Azimi-Abarghouyi and V. Fodor, "Scalable hierarchical over-the-air federated learning," *IEEE Transactions on Wireless Communications*, vol. 23, no. 8, pp. 8480–8496, 2024.

[29] ———, "Hierarchical over-the-air federated learning with awareness of interference and data heterogeneity," in *IEEE Wireless Communications and Networking Conference (WCNC)*, 2024, pp. 1–6.

[30] W. Wen, Z. Chen, H. H. Yang, W. Xia, and T. Q. Quek, "Joint scheduling and resource allocation for hierarchical federated edge learning," *IEEE Transactions on Wireless Communications*, vol. 21, no. 8, pp. 5857–5872, 2022.

[31] T. Zhang, K.-Y. Lam, and J. Zhao, "Device scheduling and assignment in hierarchical federated learning for Internet of Things," *IEEE Internet of Things Journal*, vol. 11, no. 10, pp. 18 449–18 462, 2024.

[32] Q. Ma, Y. Xu, H. Xu, J. Liu, and L. Huang, "FedUC: A unified clustering approach for hierarchical federated learning," *IEEE Transactions on Mobile Computing*, vol. 23, no. 10, pp. 9737–9756, 2024.

[33] Z. Xu, D. Zhao, W. Liang, O. F. Rana, P. Zhou, M. Li, W. Xu, H. Li, and Q. Xia, "HierFedML: Aggregator placement and UE assignment for hierarchical federated learning in mobile edge computing," *IEEE Transactions on Parallel and Distributed Systems*, vol. 34, no. 1, pp. 328–345, 2022.

[34] Q. Wu, X. Chen, T. Ouyang, Z. Zhou, X. Zhang, S. Yang, and J. Zhang, "HiFlash: Communication-efficient hierarchical federated learning with adaptive staleness control and heterogeneity-aware client-edge association," *IEEE Transactions on Parallel and Distributed Systems*, vol. 34, no. 5, pp. 1560–1579, 2023.

[35] R. A. Horn and C. R. Johnson, *Matrix Analysis*, 2nd ed. Cambridge University Press, 2013.

[36] H. Yu, R. Jin, and S. Yang, "On the linear speedup analysis of communication efficient momentum SGD for distributed non-convex optimization," in *International Conference on Machine Learning*. PMLR, 2019, pp. 7184–7193.

[37] F. Haddadpour and M. Mahdavi, "On the convergence of local descent methods in federated learning," *arXiv preprint arXiv:1910.14425*, 2019.

[38] S. Boucheron, G. Lugosi, and P. Massart, *Concentration Inequalities: A Nonasymptotic Theory of Independence*. Oxford University Press, 2013.

[39] G. Cohen, S. Afshar, J. Tapson, and A. Van Schaik, "EMNIST: Extending MNIST to handwritten letters," in *2017 international joint conference on neural networks (IJCNN)*. IEEE, 2017, pp. 2921–2926.

[40] H. Xiao, K. Rasul, and R. Vollgraf, "Fashion-MNIST: A novel image dataset for benchmarking machine learning algorithms," *arXiv preprint arXiv:1708.07747*, 2017.

[41] M. Gurbuzbalaban, U. Simsekli, and L. Zhu, "The heavy-tail phenomenon in SGD," in *International Conference on Machine Learning*. PMLR, 2021, pp. 3964–3975.

[42] U. Simsekli, M. Gurbuzbalaban, T. H. Nguyen, G. Richard, and L. Sagun, "On the heavy-tailed theory of stochastic gradient descent for deep neural networks," *arXiv preprint arXiv:1912.00018*, 2019.

[43] S. M. Kay, *Fundamentals of Statistical Signal Processing: Estimation Theory*. Prentice Hall, Inc., 1993.